Dalton Transactions

RSCPublishing

PERSPECTIVE

Processing of dielectric oxynitride perovskites for powder, ceramics, compacts and thin films

Cite this: DOI: 10.1039/x0xx00000x

Y. Masubuchi*[a], S.-K. Sun*[a], and S. Kikkawa[a]

Received 00th January 2012,
Accepted 00th January 2012

DOI: 10.1039/x0xx00000x

www.rsc.org/

Oxynitride perovskites having oxide and nitride anions together in a compound, are a new class of dielectric material. The shaping process in either the bulk ceramics or thin films is an essential factor for investigating and utilizing the dielectric properties. In this perspective, recent studies on the shaping of dielectric oxynitride perovskites are reviewed with consideration of powder preparation and thermal stability for sintering, several sintering methods, ultra-high pressure compaction, and thin-film formation.

1. Introduction

Many types of oxide crystallize with perovskite and related structures[1]. Some of these crystalline materials have been utilized in applications such as ferroelectric and piezoelectric ceramics, cuprate superconductors, non-linear optical materials and energy productions. Oxynitrides that crystallize in the perovskite structure are emerging in applications such as photocatalysis and as harmless pigments[2]. These oxynitride perovskites absorb visible light because they have a more covalent nature than oxides[3]. The anion order is an interesting structural feature that appears with oxynitride perovskites, which have both oxide and nitride anions together in the compound[2a,4]. Local ordering of nitride anions in the *cis*-configuration was reported for TaO_4N_2 octahedra in $SrTaO_2N$ and TaO_2N_4 in $RTaON_2$ (R = La, Ce, Pr)[5]. This ordering may affect the electrical, magnetic and especially the dielectric properties of oxynitride perovskites[4]. Nonstoichiometry was introduced into oxynitride perovskites, which resulted in notable electronic transport properties, such as thermoelectricity in $SrMoO_{2-x}N_{1+x}$, and colossal magnetoresistance in $EuNbO_{2+x}N_{1-x}$ and $EuWO_{1+x}N_{2-x}$[6].

The dielectric response of $BaTaO_2N$ was first deduced from the infrared reflection spectra of a pelletized polycrystalline sample[7]. Relatively large dielectric constants have also been reported for oxynitride perovskites, especially $ATaO_2N$, where A = Ba, Sr[8]. However, the dielectric properties cannot be investigated or utilized in an application without appropriate shaping, either in the bulk ceramics or thin films. Their densification was not easily achieved to maintain the chemical composition as that before sintering[2a]. They easily release a part of nitrogen from the perovskite crystal lattice of the oxynitrides to become semiconducting. Post annealing of the sintered $SrTaO_2N$ was thus required to recover the original insulating behaviour[9]. Thin-film deposition is an alternative shaping method, with techniques such as sputter deposition applied to form $LaTi(O,N)_3$ thin films[10]. Ferroelectricity was reported in compressively strained $SrTaO_2N$ thin films that were epitaxially grown on $SrTiO_3$ substrates using nitrogen plasma-assisted pulsed laser deposition[11].

Thermal stability in an oxygen-free atmosphere is an obstacle for these shaping processes. $LaTiO_2N$ partly decomposes into a mixture of La_2O_3, TiN and residual $LaTiO_2N$ in two steps at approximately 950 and 1100 °C, respectively, which releases a part of the nitrogen in the lattice[2a,12]. $SrTaO_2N$ also undergoes a two-step reaction at approximately 600 and 1200 °C. X-ray diffraction (XRD) analysis indicated the presence of unreacted $SrTaO_2N$ and a small fraction of an unidentified phase[2a,12]. Therefore, further detailed investigation is required on the thermal behaviour in relation to the sintering. The sintering of $SrTaO_2N$ using a sintering aid was investigated under a pressurized nitrogen atmosphere[9a,9c]. Hot isostatic pressing (HIP) was also applied on an encapsulated compact of $SrTaO_2N$[9b]. An ultra-high pressure compact of $SrTaO_2N$ was recently studied both at ambient and high temperatures[13]. In addition, a new synthesis method was developed to obtain $SrTaO_2N$ powder with a homogeneous particle size distribution to accelerate the densification process[14].

The thermal stability of several types of metal nitrides and oxynitrides has been well studied. Transition metal nitrides gradually become unstable with an increase in their antibonding electronic contribution[15]. For example, a powder of α"-$Fe_{16}N_2$ was prepared by ammonolysis of α-Fe powder at a very low temperature because of the thermally unstable chemical bonds between iron and nitrogen[16]. The thermal instability have proved useful for the preparation of magnetic granular thin films exhibiting useful properties such as magnetoresistance and microwave absorption[17]. The unstable nature was also effective for obtaining gallium oxynitride nanowire prepared through the citrate route[18]. Thermal stability of Ta-N chemical bond needs to be studied to overcome the thermal decomposition of $SrTaO_2N$.

The thermal stability reported for $SrTaO_2N$ in an Ar atmosphere is not consistent with the result of a study on the crystal structure against temperature. Oxide/nitride anion *cis*-ordering was expected to induce Ta cation displacement in dielectric $ATaO_2N$ (A = Sr, Ba)[5a]. The local anion order was described as forming a three-dimensional disordered zigzag Ta-N chain[5a,19]. The presence and thermal stability of anion order in the $SrTaO_2N$ and $LaTaON_2$ oxynitride perovskites was investigated using high resolution powder neutron and electron

diffraction[20]. The anion order was maintained up to 1100 °C and was expected to be stable up to significantly higher temperatures greater than 2000 °C. The structural refinement was performed without assuming any chemical compositional change, in contradiction to the previous study[12]. Approximately 1 g of each sample was vacuum sealed in a quartz tube for the measurement. The thermal stability is controversial to the thermally unstable nature of $SrTaO_2N$ and $LaTiO_2N$ investigated in an Ar atmosphere[2a,12]. The former oxynitride underwent a two-step reaction to release some nitrogen, while keeping the crystal structure of $SrTaO_2N$ up to 1200 °C. Further investigations are required to understand the high temperature behaviour of $SrTaO_2N$ and the related oxynitride perovskite crystal structures, including the nonstoichiometric chemical composition, and the physical and chemical properties. It is not obvious whether the different thermal behaviour is dependent on the experimental conditions or the accuracy of the studies.

Here, we describe the present state of oxynitride perovskite shaping for dielectric materials. Various powder preparation methods are introduced to determine a suitable method for sintering. Thermal stability is reviewed with respect to the sintering conditions. The phases determined from XRD analysis, and the microstructure and dielectric properties are discussed for the sintered body after subsequent annealing in an ammonia flow. High pressure compaction up to 8 GPa at ambient temperature was also applied to prevent the thermal decomposition of $SrTaO_2N$. The research on thin films is also reviewed and compared with that for bulk oxynitride perovskite dielectric materials.

2. Powder synthesis

Oxynitride powders with a perovskite structure have been prepared using a variety of synthesis routes. Ammonolysis of oxide precursors is the most commonly-used powder preparation method, where ammonia (NH_3) acts as a reducing agent and as a nitrogen source. The oxide precursor is prepared in advance by solid state reaction (SSR) or a soft chemistry route (SCR). The differences between the SSR and SCR methods are compared. In addition, the use of novel nitrogen sources from reactants other than NH_3 is also reviewed.

2.1. Solid state reactions

The SSR approach generally involves a two-step process, the preparation of complex oxides by calcining binary oxides in air, and subsequent ammonolysis of the as-prepared oxides to yield oxynitride products[5b,9c,21]. One typical example is the formation of $SrTaO_2N$ by the ammonolysis of a $Sr_2Ta_2O_7$ precursor, which was obtained by calcining $SrCO_3$ and Ta_2O_5 at 1200 °C in air[5b,9c]. Ammonia partially decomposes into hydrogen and nitrogen at high temperature[21e,22]. Nitrogen, hydrogen and ammonia molecules are absorbed onto the surface of the oxide precursor. Exchange occurs between the oxide anions at the surface and the adsorbed nitrogen to give nitride anions, and the oxygen is evolved as a gas by reaction with the high concentration of surface hydrogen to form water vapour molecules[21e].

A mixture of oxides and carbonates can also be used directly for nitridation in NH_3[5a,8]. For example, a mixture of $BaCO_3$ and Ta_2O_5 in a molar ratio of 2 was nitrided at 950 °C to obtain $BaTaO_2N$[8,21e]. In addition, single-crystal oxides have also been used as the precursor to produce oxynitrides on the oxide surface[23].

Temperatures ranging from 700 to 1200 °C are generally required to complete the nitridation reactions, depending on the reactivity of the oxide precursor. $SrMoO_{2.6}N_{0.4}$ and $SrMoO_{1.95}N_{1.05}$ perovskites were obtained by the nitridation of $SrMoO_4$ at 750 and 800 °C, respectively[6a,24]. However, the synthesis of pure $SrTaO_2N$ from $Sr_2Ta_2O_7$ in our previous work required a nitriding temperature of 1000 °C for 80 h, with intermittent regrinding of the products in every 20 h[5b,9c]. In addition, the complete nitridation of $Ca_2Ta_2O_7$ was more difficult, where a trace amount of $Ca_2Ta_2O_7$ still remained as an impurity, even after nitridation at 1100 °C for 240 h[8].

The key factors in this method include the gas exchange, synthesis conditions, reactivity and the surface area of the oxide precursor. Ammonolysis with intermediate regrinding is required to complete the reaction, which results in a low efficiency and tedious preparation. The addition of minerals (also called a flux), such as chloride salts of NaCl and KCl, can significantly lower the preparation temperature and shorten the total duration time for completion of the ammonolysis reaction[2c,8,25]. Ionic diffusion is thought to be enhanced significantly by the introduction of a molten medium from flux, which facilitates formation of the desired oxynitride perovskite phase in a moderate temperature range. As an example, single-phase $CaTaO_2N$ could be obtained by reaction between the intermediate phase and a NaCl/KCl flux within a shortened reaction time of 80 h[8,25a]. However, it was reported that the $CaTaO_2N$, $SrTaO_2N$ and $LaTaON_2$ oxynitrides produced by this method inevitably contained potassium as a contaminant (*ca*. 0.5 at% relative to Ta)[25a]. The contamination was confirmed by the lowered nitrogen content compared to samples obtained without the use of a flux. As a consequence, a systematic investigation and comparison of the relevant properties would be difficult using this synthesis method.

2.2. Soft chemistry routes

To enhance the efficiency of ammonolysis, SCRs have been applied to oxide precursor preparation, *e.g.*, co-precipitation and sol-gel methods[26]. Among the numbers of preparation routes, the citrate route, also known as the Pechini method, has been widely used in recent years[27]. Further heat-treatment of the precursor in NH_3 yields the target oxynitride with a high degree of homogeneity and dispersion.

In our previous work, $CaTaO_2N$ was successfully synthesized by ammonia nitridation via the citrate precursor route[28]. In comparison with the SSR, the formation of pure $CaTaO_2N$ could be achieved at 1000 °C with a reaction time of only 15 h[28]. Rachel *et al.* made a detailed comparison of the differences between oxide precursors obtained by SSR and SCR for the preparation of tantalum or niobium perovskite oxynitrides[29]. The nitridation of amorphous precursors obtained by a SCR occurred at lower temperatures and was completed within a shorter time. A relatively large surface area of 40 m^2/g and a characteristic mesoporous hysteresis were observed for the $LaTiO_2N$ sample produced through the citrate route. Gas exchange was favoured by the large surface area and high porosity of the amorphous oxide precursor, and could be ascribed to the enhanced reactivity[2a,29].

A-site solid solutions of oxynitride perovskites could be prepared using the SSR and SCR approaches. Binary complex perovskite solid solutions of $LaTaON_2$−$CaTaO_2N$ were prepared by SSR as non-toxic alternatives to cadmium-based red-yellow pigments[2c]. However, a flux was added to accelerate the nitridation[2c,25b]. A series of pure $Ca_{1-x}Eu_xTa(O,N)_3$ was successfully synthesized in the entire range of Ca/Eu

compositions via SCR, which demonstrates its advantage over SSR[28,30].

2.3. Direct synthesis

During nitridation at high temperature, the as-generated hydrogen from NH_3 is likely to react with the as-prepared oxynitrides, which results in a reduced oxidation state of the B-site transition metals. These undesired side reactions can be avoided if only nitrogen is used during nitridation. The use of alternative nitrogen sources, instead of NH_3, has been developed in recent years. For example, oxynitride perovskites were prepared by the urea route, according to ref. 31. Urea decomposed at 550 °C according to $CO(NH_2)_2 \rightarrow NH_3 + HCNO$, which provides NH_3 for subsequent nitridation of the oxide precursor. However, if excess urea is mixed with the raw materials, then it is possible that carbon residuals remain in the product, which would be problematic. On the other hand, some metal (oxy)nitrides could be used as the raw material to obtain oxynitride perovskites. Nd_2AlO_3N was prepared by the reaction of AlN and Nd_2O_3 at 1350 °C[32]. A high temperature is generally required for complete reaction; therefore, an additional N_2 atmosphere is typically employed to inhibit thermal decomposition of the oxynitride product.

A high-temperature synthesis was explored by Clarke *et al*[33]. $ATaO_2N$ powder (A = Ba or Sr) was obtained through the direct reaction of the alkaline earth oxide and TaON at 1500 °C under a N_2 atmosphere rather than under NH_3. While the product was phase pure according to an XRD analysis, it was nonstoichiometric $SrTaO_2N$ with a brown colour, rather than the orange coloured stoichiometric composition of $SrTaO_2N$ obtained by SSR or SCR.

A facile direct synthesis was recently developed to prepare $ATaO_2N$ (A = Ca, Sr and Ba) by the reaction of Ta_3N_5 and the alkaline earth carbonate in N_2[14a]. The evolution of a mixed gas containing CO, CO_2 and N_2 was observed during the heat treatment. The reaction mechanism for $SrCO_3/Ta_3N_5$ was described as follows: $SrCO_3$ dissociates into SrO and CO_2, which serve as a strontium source and an oxidizing agent, respectively. The reaction between Ta_3N_5 and CO_2 may induce the formation of TaON, which subsequently reacts with SrO to form $SrTaO_2N$, on the basis of the high-temperature synthesis.

$$Ta_3N_5 + 3CO_2 \rightarrow 3TaON + 3CO\uparrow + N_2\uparrow$$
$$SrO + TaON \rightarrow SrTaO_2N$$

It should be noted that the formation temperature for $SrTaO_2N$ was significantly lowered to 950 °C, compared with 1500 °C employed for the high-temperature synthesis, and stoichiometric oxygen and nitrogen contents were observed on the resultant $SrTaO_2N$. Furthermore, the as-synthesized $SrTaO_2N$ powder product (Fig. 1a) contained quasi-spherical particles with an average size of 330 nm, with a sharp particle size distribution. Nevertheless, Fig. 1b shows that $SrTaO_2N$ powder prepared by the SSR method had an inhomogeneous particle size distribution with a slightly larger particle size. A list of the above mentioned synthesis methods for oxynitride perovskites is given in Table 1.

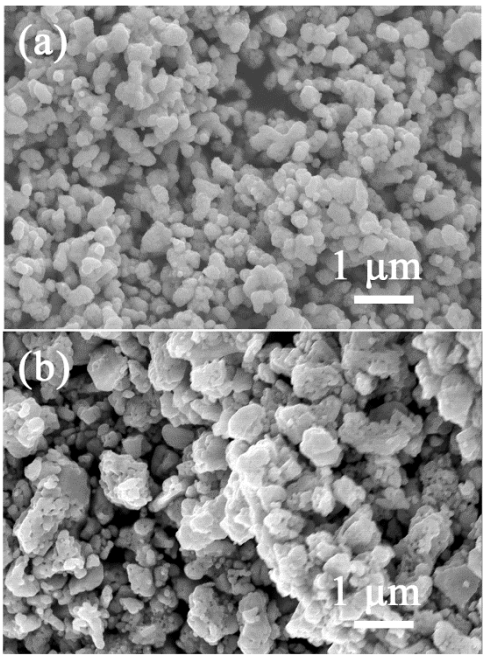

Fig. 1 SEM images of $SrTaO_2N$ powder produced by (a) direct synthesis at 950 °C in N_2 and by (b) SSR at 1000 °C in NH_3. Reproduced with permission from ref. 14a. Copyright 2014 Elsevier.

2.4. Thermal Stability

Investigation of the thermal oxidation of ABO_2N (A = Ca, Sr, Ba; B = Nb and Ta) oxynitride perovskites in an oxygen-containing atmosphere revealed the presence of dinitrogen (N≡N) loosely bound to B and N≡B bonds (B = transition metal) in the intermediate compounds, and the corresponding oxides were formed at high temperatures of 800–1000 °C[12,29].

The low thermal stability of oxynitride perovskites is an obstacle for the shaping/sintering processes in an oxygen-free atmosphere. According to refs. 29 and 34, the thermal decomposition of $LaTiO_2N$ consists of two steps at around 950 and 1100 °C, with the release of nitrogen. A mixture of La_2O_3, TiN and residual $LaTiO_2N$ was detected in the decomposition product. For $SrTaO_2N$, it was found that the decomposition mixture consisted of $SrTaO_2N$ and an unidentified phase[12]. The colour of the product after decomposition in an Ar atmosphere was black, which suggested that the oxidation state of Ta decreased after thermal decomposition.

Thermal decomposition has a serious effect on the sintering characteristics. $SrTaO_2N$ powder produced by SSR was studied to eliminate the influence of residual carbon (possibly originating from the SCR or the graphite furnace). Two weight losses were observed for $SrTaO_2N$ at below 650 and above 1150 °C during heating in a flow of Ar, as shown in Fig. 2, which is similar to the result from ref. 12. Thus, thermal decomposition with the release of nitrogen from $SrTaO_2N$ appears to be inevitable if the sintering is conducted at temperatures above 1200 °C.

Table 1 Powder synthesis of oxynitride perovskites

Compound	Synthesis method	Ref.
Solid state reactions (SSR)		
$SrTaO_2N$	$Sr_2Ta_2O_7$, NH_3, 950-1000 °C	5b, 8
$SrTaO_2N$ (nano)crystal	$Sr_2Ta_2O_7$ crystal, NH_3, 950 °C	23
$BaTaO_2N$	$BaCO_3/Ta_2O_5$, NH_3, 950 °C	8, 21e
$SrMoO_{2.6}N_{0.4}/SrMoO_{1.95}N_{1.05}$	$SrMoO_4$, NH_3, 750/800 °C	6a, 24
$CaTaO_2N$	$Ca_2Ta_2O_7$, NH_3, 1100 °C	8
$Ca_{1-x}La_xTaO_{2-x}N_{1+x}$ solid solution	$CaCO_3/La_2O_3/Ta_2O_5$ + flux ($CaCl_2$, KCl, NaCl), NH_3, 850 °C	2c
Soft chemistry methods (SCR)		
$Ca_{1-x}Eu_xTa(O,N)_3$	Ca-Eu-Ta-O (citrate), NH_3, 1000 °C	28
$LaTiO_2N$	La-Ti-O (Pechini), NH_3, 950 °C	2a
ABO_2N (A = Ca, Sr, Ba, B = Nb, Ta)	A-B-O (A = Ca, Sr, Ba, B = Nb, Ta) (citrate), NH_3, 750 °C (Nb), 950 °C (Ta)	29
Direct synthesis		
ABO_2N (A = Ca, Sr, Ba, B = Ta, Nb)	ACO_3 (A = Ca, Sr, Ba)/B_2O_5 (B = Nb, Ta) + excess urea, N_2, 850 – 950 °C	31
$ATaO_2N$ (A = Sr, Ba)	AO (A = Sr, Ba)/TaON, N_2, 1500 °C	33
$ATaO_2N$ (A = Sr, Ba)	ACO_3 (A = Sr, Ba)/Ta_3N_5, N_2, 950 °C (Sr), 850 °C (Ba)	14a, 14b
$CaTaO_2N$	$CaCO_3$/TaON, N_2, 1000 °C	14b

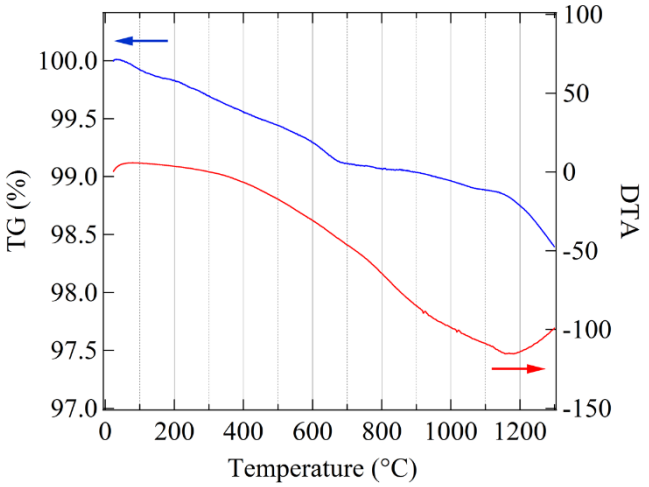

Fig. 2 TG and DTA curves for $SrTaO_2N$ in Ar flow.

$SrTaO_2N$ powder produced by SSR was isolated in a vacuum-sealed quartz tube and heat-treated at 1200 °C[9c]. The main phase was determined to be $SrTaO_2N$ with a $TaO_{0.9}$ impurity, and the colour of the product was changed to brown. Besides, the nitrogen content in the samples had decreased obviously after firing at 900 and 1000 °C. These results indicate that the crystal structure of $SrTaO_2N$ is likely to change after heating at 1200 °C with the partial loss of Sr (or SrO) and nitrogen from the compound, which should be compensated to maintain the original composition during the fabrication of ceramics. On the other hand, the anion order of $SrTaO_2N$ as a function of temperature was investigated using high resolution neutron and electron diffraction[20]. No loss of anion order was observed up to 1100 °C and the order was expected to remain stable at temperatures as high as 2000 °C[20]. These contrasting results indicate that further investigations are required to understand the crystal structures of partially-decomposed $SrTaO_2N$ and the related oxynitride perovskites, including the nonstoichiometry, and the physical and chemical properties.

3. Sintering and dielectric properties

Bulk samples are necessary for measuring the dielectric properties and also for dielectric applications. However, due to the low thermal stability, oxynitride perovskites are rather difficult to densify while maintaining the chemical composition and crystal structure. In this section, the sintering methods and the dielectric properties of bulk oxynitrides are discussed.

3.1. Sintering in ammonia

As an expedient method, the sintering of oxynitrides in ammonia was featured by preparation of a green body under high pressure (*e.g.*, 760 MPa), and subsequent heat treatment at a moderate temperature in NH_3. Although considerable porosity remained, the pellet had sufficient mechanical strength and electrical conductivity pathways necessary for characterization. $SrMoO_2N$ bars were obtained by cold isostatic pressing at 200 MPa and subsequent sintering under flowing NH_3 at 800 °C[6a]. The relative density (RD) of the bars varied between 74% and 89% of the theoretical value. The $SrMoO_2N$ oxynitride showed semiconducting resistivity behaviour in contrast to its parent metallic oxide, $SrMoO_3$. Similarly, $EuWO_{1+x}N_{2-x}$ and $EuTaO_2N$ compacts with diameters of 7 mm were prepared under a high pressure of 760 MPa and subsequently sintered in NH_3[6d,6e]. $EuTaO_2N$ was highly insulating and the electrical resistivity was too large to be measured at low temperature ($\rho > 10^9$ Ω·cm below 165 K). The low temperature (<165 K) dielectric constant of $\varepsilon_r = 37$ had a slight frequency dependence[6e].
Kim *et al.* prepared compacts of $ATaO_2N$ (A = Ba, Sr, Ca) by a stepwise process that involved uniaxial pressing (206 MPa) of the powdered oxynitride samples, followed by cold isostatic pressing (412 MPa), and then heating under flowing NH_3 at 1020 °C for 2 h[8]. The resultant samples had a RD of around 55%. The measured impedance spectra for the $BaTaO_2N$ and $SrTaO_2N$ compacts were composed of two semicircles, which represent the bulk and grain boundary resistance contributions. The dielectric permittivities (ε_r) of $BaTaO_2N$ and $SrTaO_2N$ were derived from an equivalent circuit analysis. Both compounds possessed very high ε_r values in the order of 3000–5000. The total resistivity of the $BaTaO_2N$ and $SrTaO_2N$

compacts were *ca.* 200 kΩ at room temperature. The dielectric losses for $BaTaO_2N$ and $SrTaO_2N$ were reported to be very high, at around 6.0 and 0.2 for measurements at 1 kHz and 1 MHz, respectively. The conductivity of *ca.* 10^{-5} S/cm and the relatively high porosity of the sintered pellets are likely to contribute to the high dielectric loss. An even larger bulk dielectric permittivity of 7300 was reported for $BaSc_{0.05}Ta_{0.95}O_{2.1}N_{0.9}$ with a partial substitution of Ta in $BaTaO_2N$ with Sc. However, the $CaTaO_2N$ sample with a similar RD possessed a significantly lower relative permittivity, $\varepsilon_r \approx 30$, and was highly insulating with $\sigma_{el} \approx 10^{-8}$ S/cm. To explain the origin of the high dielectric constant of $BaTaO_2N$, local dipole moments due to differences in the Ta-N and Ta-O distances were discussed[35]. A much smaller dielectric constant of *ca.* 200 was observed for $BaTaO_2N$ thin films[36] (which will be discussed later in the thin-film section). In addition, a comparison between $BaTaO_2N$ and $BaTiO_3$ was conducted using infrared reflection spectroscopy and the dielectric response of $BaTaO_2N$ was found not to reach very high values[7]. The high dielectric permittivity of $BaTaO_2N$ and $SrTaO_2N$ should be carefully studied using dense samples produced by other shaping methods, such as conventional pressureless sintering or thin-film growth.

3.2. Pressureless sintering

Conventional pressureless sintering was a subject in the subsequent investigation on dielectric oxynitride perovskite, with an emphasis on the $SrTaO_2N$ perovskite. The high-temperature processing applied in the sintering and the poor thermal stability of oxynitrides (as described in Section 2) means that pressurized nitrogen and sintering additives are generally employed to maintain the chemical composition of $SrTaO_2N$ ceramics. The pressureless sintering procedure for the oxynitride perovskite, $SrTaO_2N$ is outlined in Fig. 3.

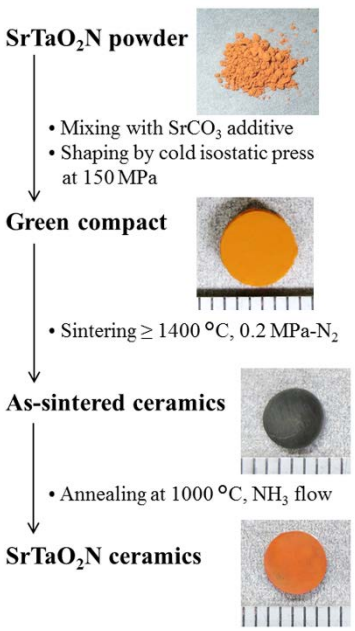

Fig. 3 Procedure of the pressureless sintering for $SrTaO_2N$ ceramics[9a,9c].

A tantalum carbide impurity appeared after sintering $SrTaO_2N$ powder produced by SCR without additives[9a]. Pure $SrTaO_2N$ ceramic with a RD of 93% could be obtained after sintering with 5 wt% $SrCO_3$ at 1400 °C. It should be noted that the as-sintered $SrTaO_2N$ ceramics were electrically conductive, mainly due to the anion vacancies in the samples. As a result of nitrogen loss at high temperature, anion vacancies are likely to be formed, which was confirmed by the change in the colour to black with sintering. To remove the anion vacancies and also recover the insulating behaviour of the samples, successive annealing in ammonia was conducted, and the resistance of the annealed samples was larger than that of the as-sintered samples by several orders of magnitude. The apparent dielectric constant for the annealed sample was as high as 10^4, which is even larger than those for oxynitride bulks obtained by ammonia sintering. The colossal dielectric constants may be associated with partial recovery of the insulating nature in the sintered body by annealing. The recovery of insulating behaviour was significantly affected by the dense morphology of the sample. Therefore, the effect of the annealing on the recovery of insulating character was carefully investigated in our recent work[9c].

To minimize the compositional change/loss during sintering in a graphite furnace, $SrTaO_2N$ powder produced by SSR was used as the starting material and $SrCO_3$ was added to compensate the SrO loss[9c]. Pure as-sintered ceramics were fabricated with 2.5 wt% $SrCO_3$ additive, as confirmed by XRD analysis. These samples with various relative densities were annealed in NH_3 to observe the recovery of colour and the electrical insulating properties. It was observed that the colour and insulating character of the inner part of the well-sintered samples with RD = 95.1% could not be completely recovered in the annealing process, and they continued to exhibit semiconducting behaviour and a black colour. The apparent dielectric constant for these samples was *ca.* 9000, which was comparable with that previously obtained. It could be speculated that the apparently high dielectric constant for $SrTaO_2N$ was non-intrinsic, but mainly due to experimental artefacts[37]. Thus, as in-depth analysis of the frequency and temperature-dependent dielectric response with different types of contacts is required for a better understanding.

On the other hand, for the as-sintered $SrTaO_2N$ ceramics with RD < 84%, the entire body of the ceramic was annealed completely back to an orange colour. The cell volume and especially the *c*-axis parameter decreased from c = 8.080 Å (V = 262.5 Å^3) to 8.072 Å (262.3 Å^3) after sintering, and then recovered to 8.079 Å (262.6 Å^3) with annealing in NH_3. The amount of nitrogen decreased to 3.77 wt% after sintering and was recovered to 4.20 wt% by annealing. The chemical composition of the annealed sample was close to the theoretical value for $SrTaO_2N$.

A small single arc was observed on a Cole-Cole plot of the as-sintered $SrTaO_2N$ ceramic with RD = 84.0%, which indicates the porous ceramic possessed a total electrical resistivity of less than 100 kΩ, similar to that reported in ref. 8. It is noteworthy that only a portion of the arc was observed after annealing, which indicates the highly insulating behaviour was recovered in the annealed ceramic. Figure 4 shows that the dielectric constants were 65 and 150 for the fully annealed ceramics with a respective RD of 55.0% and 64.0%. The dielectric constant was further increased to 320 and 450 with increasing RD of 77.3% and 83.3%. Moreover, the dielectric constant was weakly dependent on the frequency. The dielectric loss was significantly decreased to values less than 0.1 and 0.07 at 100 Hz and 10 kHz, in comparison to the previously reported values for $SrTaO_2N$ compacts prepared by sintering in NH_3[8].

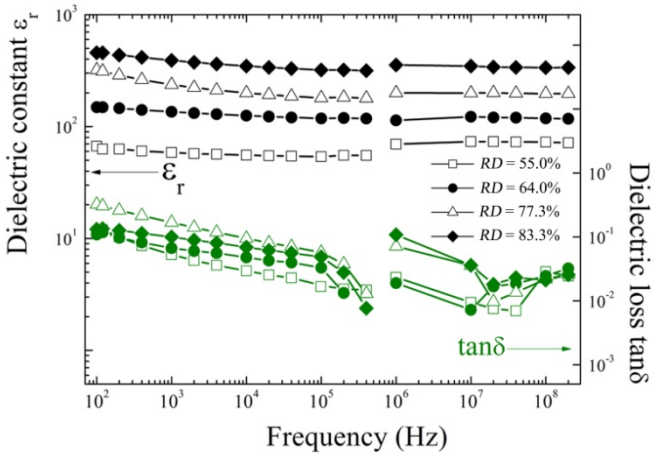

Fig. 4 Dielectric constant and dielectric loss versus frequency at room temperature for annealed $SrTaO_2N$ ceramics with various relative densities. Reproduced with permission from ref. 9c. Copyright 2014 John Wiley and Sons Ltd.

The sinterability of the $SrTaO_2N$ powders obtained by direct synthesis and by SSR was compared[14a]. In contrast to that obtained with SSR, the sinterability was enhanced for the powder prepared by direct synthesis, due to the smaller particle size; the RD value was 84.1% and 95.5% after sintering at 1400 °C for 3 and 6 h, respectively. Complete recovery of the insulating behaviour was only achieved by annealing the porous bulk samples, similar to the case of the SSR powder. The presence of pores contributed to the full recovery of the insulating nature by annealing in NH_3. The annealed $SrTaO_2N$ with RD = 82.8% had a relatively large dielectric constant of *ca.* 300 at 100 Hz and a weak dependence on the frequency, which was consistent with the results reported in ref. 9c.

3.3. Special sintering technique

It is a challenge to fabricate dense oxynitride ceramics with a stoichiometric composition. The partial composition change especially the loss of N is assumed to be suppressed if the sintering temperature were lowered. To date, special sintering techniques such as spark plasma sintering (SPS) and HIP have been applied to densify oxynitride perovskites.

Li *et al.* prepared $LaTiO_2N$ ceramics by SPS and found that the decomposition of $LaTiO_2N$ was accelerated in a vacuum, particularly in the presence of a graphite die[34]. XRD investigations showed that all the sintered compacts were crystalline $LaTiO_2N$ with La_2O_3 and TiN impurities. Under optimal conditions, a sample with 93% purity and a RD of 74% was obtained after sintering at 1250 °C and under a pressure of 75 MPa. Partial decomposition inevitably occurred, which was confirmed by the nitrogen content of 4.61wt% (theoretical value of 6.01 wt% in $LaTiO_2N$). The presence of the TiN impurity leads to (semi-)conductive behaviour and extrinsic dielectric performance.

Densification has been realized by applying HIP to encapsulated Si_3N_4 compacts[38]. Some attempts to prepare dense $SrTaO_2N$ ceramics have been made by application of a similar HIP technique[9b]. Green compacts of $SrTaO_2N$ without additives were encased within Pt sheets and then vacuum-sealed in glass capsules. Bulk consolidation was conducted under an Ar pressure of 196 MPa at 1200–1600 °C. It was confirmed that HIP at 1200 °C in an evacuated glass capsule was effective for suppressing the Sr loss observed with conventional pressureless sintering. A trace amount of impurity, which could be a TaC-related species, was detected in the $SrTaO_2N$ sample prepared at 1400 °C. The carbide impurity was assigned to contamination with amorphous carbon in the starting powder synthesized through the citrate route. However, the impurity disappeared after annealing in NH_3. $Sr_2Ta_2O_7$ and $Ta_{1.1}O_{1.05}$ impurities were evident in the product obtained after sintering at 1600 °C, and these impurity phases remained even after annealing.

The RD of $SrTaO_2N$ bulk HIP-sintered at 1200, 1400 and 1600 °C were 90, 82 and 86%, respectively. All the bulk samples changed colour from brown to dark grey after HIP sintering, which was very similar to the pressureless sintered bodies with anion deficiencies in the crystal lattice[9c]. Annealing in ammonia returned the colour of the sample sintered at 1400 °C to brown, probably due to supplementation of the anion deficiency. However, the annealing treatment was unsuccessful for the samples sintering at 1200 and 1600 °C and the sample remained a dark grey colour, even after annealing. This was attributed to the dense microstructure with compacted grains of the as-sintered ceramics. The apparent dielectric constant for the $SrTaO_2N$ ceramic sintered at 1400 °C was very high and was 7800 at 100 Hz. More investigations are required to determine whether the entire material has been completely annealed or not.

The questions in the fabrication of dense bulk samples with original composition must be addressed, so that the intrinsic properties of oxynitride perovskites can be measured with confidence. Anionic local configuration for the bulk ceramics also need to be addressed in relation to the sintering process. Neutron diffraction analysis for the partially nitrogen released and the post-annealed $SrTaO_2N$ ceramics is under consideration. The property measurement trials were performed on thick layers of $LaTiO_2N$, $NdTiO_2N$, $SrNbO_2N$ and $SrTaO_2N$ prepared by nitridation of the corresponding oxide single crystal surfaces[39]. Further investigation is required to realize the densification of oxynitride perovskites with maintaining of the chemical composition from the two following aspects. Firstly, micro- or even nanosized powders of oxynitrides with high sinterability should be prepared. Secondly, new sintering additives should be introduced to compensate for the compositional losses (*e.g.*, Sr and nitrogen in the $SrTaO_2N$ case), and also to induce liquid-phase sintering at relatively low temperatures. The reliable fabrication of thin films is also necessary, as addressed later in Section 5.

4. High-pressure process for oxynitride perovskite

A high-pressure process of gigapascal order is useful for synthesizing new compounds containing multi-anions and for enhancing densification of materials. Such high pressure is usually generated with a multi-anvil press, belt-type high pressure apparatus, and diamond anvil cell. In this section, the synthesis of oxynitride perovskite under high pressure is reviewed. High-pressure compaction of thermally unstable $SrTaO_2N$ perovskite using a belt-type high pressure apparatus is also investigated in relation to the phase stability.

4.1. High-pressure synthesis of oxynitride perovskite

High-pressure synthesis has significant effects that cannot be achieved with conventional synthesis conditions under ambient pressure. Such effects are generally useful for forming a perovskite structure that cannot be produced at ambient pressure. Large anions, such as N^{3-} and O^{2-}, are more compressive than small cations under high pressure. High pressure also stabilizes larger coordination numbers of the constituent cations, more so than that under ambient pressure[40]. There has been much research on ternary oxides crystallized in the perovskite structure under high pressure[41]. For example,

perovskite-type $MgGeO_3$ and $ZnGeO_3$ have been synthesized from their ilmenite phases under high pressures above 20 GPa[41c]. The coordination number of cations in the ilmenite structure ($LiNbO_3$ type lattice) is 6, are increased to 8 for Mg^{2+} and Zn^{2+} under high pressure and high temperature. An increase in the coordination number for PbO and ZnO starting oxides, was also observed in the synthesis of perovskite-type oxide $Pb(Zn,Nb)O_3$ under high pressure[41a]. This approach has also been valid for mixed anion compounds containing N^{3-}, O^{2-}, and F^- together under high pressure[42]. High pressure synthesis of perovskite-type oxynitride has been reported for $BaNbO_2N$, which was prepared from a mixture of BaO, Ba_2O and NbN at 1000 °C under a high pressure of 5 GPa[43]. In the literature, perovskite-related oxynitrides such as La_2VO_3N and La_2AlO_3N, which crystallize in K_2NiF_4-type structure, have also been prepared under a high pressure of 5 GPa at 1200 °C[43]. However, $BaNbO_2N$ had also been obtained by the commonly-used ammonolysis reaction of oxide precursors at ambient pressure[8,44]. Rare-earth zirconium oxynitrides $RZrO_2N$ (R = Pr, Nd, and Sm) that adopt the perovskite structure have been obtained only by direct SSR under high pressure[45]. Mixtures of R_2O_3 and Zr_2ON_2 were reacted at 1–10 GPa and 900–1300 °C. Below 6 GPa, $RZrO_2N$ perovskite appeared in the products together with impurity phases of pyrochlore-type phases and a small amount of ZrN. These three perovskite oxynitrides adopt an orthorhombic structure having a space group of *Pnma*. The decrease in the ionic radius of R^{3+} (from Pr^{3+} to Sm^{3+}) increases the deformation and tilting of the ZrO_4N_2 octahedra, which results in the orthorhombic structural distortion. However, the products obtained at pressures above 6 GPa were mixtures of ZrN and the constituent metal oxides. The formation of perovskite-type $RZrO_2N$ oxynitrides has mainly been enhanced by the suppression of nitrogen loss under the reaction conditions below 6 GPa, rather than by an increase in the coordination number of the metal cations.

Transition metal nitrides are easily decomposed and release nitrogen at high temperature under ambient pressure. To use such thermally unstable nitrides as reactants, high-pressure synthesis allows the reaction temperature to be elevated far beyond the decomposition temperature at ambient pressure. Spinel-type gallium oxynitride was prepared at 1250 °C and 5 GPa or at 1100°C and 7 GPa using a multi-anvil high pressure apparatus[46]. The reaction temperatures were much higher than the decomposition temperature for GaN (870 °C at 1 atm of N_2)[47]. On the other hand, the decomposition of thermally unstable compounds that release nitrogen gas at high temperature can also be applied to form a very high-pressure N_2 atmosphere in a high pressure capsule. Cubic GaN nanoparticles have been obtained from Ga metal and sodium azide (NaN_3) which was decomposed in a spherical nickel capsule at 400–700 °C and 0.8 GPa in a belt-type high pressure apparatus to produce a nitrogen gas pressure of 330 MPa[48]. The use of high oxygen pressure produced by a decomposition of metal peroxides in a high-pressure capsule has been well established rather than nitrogen gas and novel perovskite oxides consisting of an abnormally high valence transition metal, such as Fe^{4+}, have been successfully synthesized[49]. High-pressure synthesis has been applied to the formation of many types of compounds. However, little research has been conducted on the application of this technique to the synthesis of oxynitrides. Significant advantages in high-pressure synthesis are expected, which makes this is a promising approach to the preparation of novel oxynitride perovskites.

4.2. High-pressure compaction of oxynitride perovskite

High-pressure conditions favour reactions decreasing a *volume* of unit cell and high-pressure compact. Denser polymorphs are stabilized under high pressure, such as in the formation of diamond and cubic BN[50]. High-pressure has also been applied to sinter many types of compounds, such as diamond, SiC, Si_3N_4, FeN_x and cubic-BN, due to their thermal instability and poor sinterability at ambient pressure[51]. However, pressure-induced phase decomposition into mixed metal compounds has also been reported when the assemblage of decomposition compounds is denser than the parent compound. The high-pressure perovskite oxide $FeTiO_3$ decomposes into a mixture of FeO and TiO_2 at high pressures above 67 GPa[52]. High-pressure deformation of zirconium oxynitride, $Zr_7O_{11}N_2$, was also reported to form a mixture of ZrO_2 and rock-salt type ZrN at 5 –6 GPa and 727 °C[53]. Only sintering of TaON has been investigated under high pressures of 3 and 5 GPa at temperatures above 900 °C using a belt-type high-pressure apparatus; however, a Ta_2O_5 impurity phase appeared at a high temperature of 1200 °C[54].

High-pressure densification of $SrTaO_2N$ perovskite was recently investigated under pressures of several gigapascals and at temperatures below 1000 °C using a belt-type high-pressure apparatus to avoid thermal decomposition[13]. The RD of the $SrTaO_2N$ compact pressed at 2.5 GPa was 64%, which was increased to 75% at 7.7 GPa without sample heating. Along with densification, the colour of the compacts changed from orange for the original $SrTaO_2N$ powder to brown and the crystallinity was decreased, as evident from line broadening in the XRD pattern. Microstructural observations of such compacts using transmission electron microscopy indicated the formation of nanoparticles due to grain fracture during high-pressure compaction, while the crystalline perovskite structure was retained, as no amorphous halo pattern was observed in the electron diffraction pattern. Heating above 800 °C at 7.7 GPa increased the density up to 85%, accompanied by a slight contraction of the unit cell. The colour of the ceramics changed to black when sintered above 800 °C at 7.7 GPa, as shown in Fig. 5. The electrically conductive characteristics were confirmed by AC impedance measurements and suggest a partial loss of nitrogen. A sintered pellet that was electrically conductive and black in colour was also obtained by sintering $SrTaO_2N$ with a small amount of $SrCO_3$ additive above 1300 °C under a 0.2 MPa of N_2 atmosphere[9a,9c]. The sintered pellet showed a slight decrease in the *c*-axis lattice constant of the crystal due to a partial loss of nitrogen. TaO also appeared as an impurity phase when $SrTaO_2N$ was thermally decomposed above 1100 °C in vacuum. $SrTaO_2N$ has a theoretical density of 7.9 g/cm^3, which is lower than that for rock-salt type tantalum monoxide TaO, and mononitride TaN, with a theoretical density of around 15 g/cm^3 [5b,55]. Such a denser phase may be more stable than $SrTaO_2N$ under high pressure. Decomposition may occur with high-pressure sintering above 800 °C, which is 300 °C lower than the temperature of thermal decomposition observed in Ar flow and under vacuum as described in the above section 2.4[9c,12]. The presence of a denser phase than $SrTaO_2N$ may reduce the stability of the perovskite oxynitride phase at high pressure. On the other hand, a $SrTaO_2N$ compact heated at 600 °C under 7.7 GPa having a RD of 75%, maintained highly insulating behaviour during impedance analysis and exhibited a permittivity of 210 and dielectric loss of 0.4 at 100 Hz at room temperature.

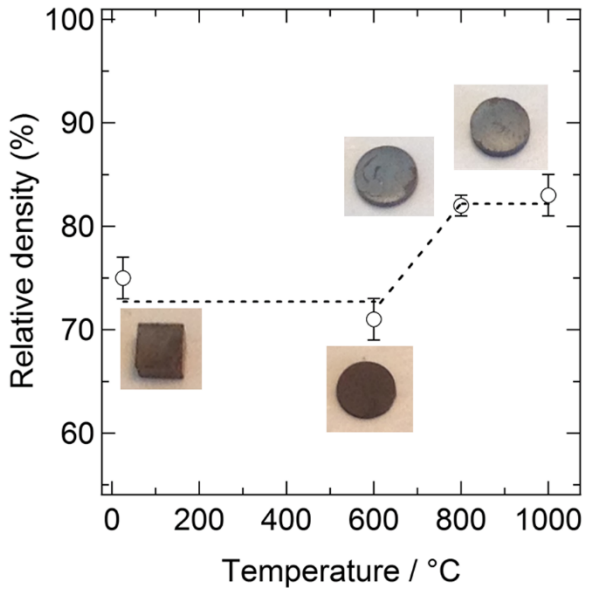

Fig. 5 Relative density of high-pressure $SrTaO_2N$ compacts as a function of the heating temperature when prepared under 7.7 GPa. Inset images show the colours of the compacts. Reproduced with permission from ref. 13. Copyright 2014 Elsevier.

Little research has been conducted on the synthesis or densification of oxynitride under pressure of gigapascal order. High-pressure processing may be useful for synthesizing and densifying oxynitrides due to a suppression of nitrogen loss at high temperature and also by the stabilization of new perovskite structures with higher coordination numbers than in the raw materials. However, pressure-induced decomposition was observed at higher pressures and temperatures due to the formation of denser crystalline phases, such as rock-salt type tantalum oxide or nitride.

5. Thin film of oxynitride perovskite

The formation of oxynitride perovskite bulk ceramics has been reviewed in the previous sections to study the dielectric properties. Fabrication of thin films is another method of shaping materials that are different from bulk ceramics. In this section, two thin-film deposition methods, sputter deposition and pulsed laser deposition, are reviewed in terms of thin-film formation and the resultant electrical properties.

5.1. Sputter deposition of oxynitride perovskite

Thin films of $BaNbO_xN_y$ and $LaNbO_xN_y$ perovskite oxynitrides were prepared by reactive sputtering using multi-phase targets of mixed powder compacts, Ba_3N_2 + 3NbN and LaN + NbN, instead of an oxynitride target due to difficulty in the preparation of the sintered oxynitride target[56]. Crystalline $BaNbO_{1.65}N_{1.24}$ was obtained under a sputtering gas of 70% N_2 + 30% Ar; however, the $LaNbO_{0.29}N_{2.48}$ formed was amorphous. The lattice parameter for the cubic perovskite $BaNbO_{1.65}N_{1.24}$ was slightly larger than that for bulk $BaNbO_2N$, due to the nonstoichiometry in the O:N ratio, and a relatively low electrical resistivity of 4×10^3 Ω·cm was observed. For a dielectric perovskite oxynitride, nonstoichiometry in the O:N ratio should be avoided, due to the formation of conductive *d* electrons, to maintain the insulating behaviour. Reactive sputter deposition of oxynitride perovskites has been further developed by a French group in respect to the O:N ratio[10a,10b]. Perovskite-type $LaTiO_xN_y$ thin film was epitaxially grown on $SrTiO_3$ and MgO single crystal substrates at 750–900 °C using a $LaTiO_2N$ target obtained by uniaxial pressing at 32 MPa in Ar-N_2 reactive plasma gas. The nitrogen content of the thin films was changed between 0 and 20 at% according to the substrate temperature and the Ar/N_2 ratio. The dielectric properties of the stoichiometric $LaTiO_2N$ thin film were reported to be $\varepsilon_r \approx 140$ with a low dielectric loss of 0.012 at 100 kHz and $\varepsilon_r \approx 170$ with a loss of 0.011 at 12 GHz[57]. Recently, both electrical tuning properties and photoelectrodes for water splitting have been investigated using sputter deposited $LaTiO_2N$ thin films[10c,10f,58].

5.2. Pulsed laser deposition of oxynitride perovskite

In contrast with sputter deposition, the pulsed laser deposition method was applied to prepare thin films of $AETaO_2N$ (AE = Ca, Sr, and Ba), $LaTiO_2N$, and $(La,Sr)Ti(O,N)_3$ perovskite oxynitrides[11,36,59]. A phase-pure $BaTaO_2N$ thin film was epitaxially grown by pulsed laser deposition from a $BaTaO_2N$ target onto a $SrRuO_3$ buffer layer on a $SrTiO_3$ single-crystal substrate under a strictly controlled gas mixture of N_2 and O_2 in a reactive chamber[36]. The $BaTaO_2N$ thin film was tetragonally distorted to have a *c/a* ratio of 1.009, as confirmed with a three-circle X-ray diffractometer. The distortion was considered to be due to compressive stress from the lattice mismatch between $BaTaO_2N$ and the $SrRuO_3$ buffer layer. The 600-nm-thick $BaTaO_2N$ thin film had a dielectric permittivity around 230 with small temperature and frequency dependence. The dielectric permittivity is one order of magnitude smaller than that observed for incompletely sintered $BaTaO_2N$ compacts with a low RD of *ca.* 55%[8]. However, the dielectric permittivity is almost comparable to that for a well-sintered $SrTaO_2N$ ceramic ($\varepsilon_r \approx 450$) and high-pressure $SrTaO_2N$ compact ($\varepsilon_r \approx 210$).

Recently, ferroelectric nanodomains in a relaxor-type matrix were reported for a $SrTaO_2N$ thin film obtained by nitrogen-assisted pulsed laser deposition on a $SrTiO_3$ substrate[11]. The dielectric constant for the $SrTaO_2N$ thin film was around 2000 and increased with the measurement temperature. The dielectric constant is comparable with that for incompletely sintered $SrTaO_2N$[8]. The positive thermal dependence $d\varepsilon_r/dT$, implies intrinsic relaxor-type dielectric properties for the majority of $SrTaO_2N$ thin film. Surrounded by a relaxor-type matrix, the nanosized domains exhibit ferroelectric behaviour, as observed using piezoresponse force microscopy. The ferroelectricity of the nanodomains has been considered to occur in compressively strained $SrTaO_2N$ with a *trans*-type O/N distribution, as suggested by first principle calculations[11]. The characteristic dielectric properties and the anion ordering have not been reported for either bulk or powder oxynitride perovskites. Thin films epitaxially grown on a crystalline substrate typically have a lattice mismatch with the underlying substrate. Therefore, local stress is expected to have an effect on the local crystal structure and electrical properties.

The functionality of oxynitride perovskites may be controlled by modifying the anionic arrangement by exploiting the epitaxial lattice mismatch. However, the intrinsic properties of oxynitride perovskite thin films are not yet fully understood. Studies on thin films formed with and without the influence of lattice mismatch from various substrates and buffer layer materials are required in order to investigate the anion-controlled dielectric properties of oxynitride perovskite thin films.

6. Conclusions

Oxynitride perovskites are attractive dielectric materials because their properties can be modified according to the oxide/nitride anionic ratio and the distributions of these anions in the compounds. The shaping of these oxynitrides, either in dense sintered ceramics or in thin films, is necessary for studying the dielectric properties and developing practical applications. Many powder preparation methods have been applied to produce a suitable morphology for sintering. A new ammonia-free process was also developed to achieve a homogeneous particle size distribution. Both $SrCO_3$ as a sintering additive and annealing in ammonia have proven to be effective for compensating for the partial composition loss during the sintering of $SrTaO_2N$. Annealed $SrTaO_2N$ with a RD of 83.3% had a dielectric constant of 450 at 100 Hz with weak frequency and temperature dependency. Ultra-high pressure compaction at pressures up to 7.7 GPa and at ambient temperature has realized dense $SrTaO_2N$ compacts with a RD of 75% without thermal decomposition. Thin-film formation is another material shaping method, and sputter and pulsed laser depositions have been mainly used to prepare dielectric oxynitride perovskite thin films. In many studies on oxynitride perovskites, *intrinsic* dielectric behaviour has been approached, but not yet achieved. Further research to achieve the fabrication of dense ceramics without compositional change and to produce thin films without influence from the substrate will lead to a better understanding of the *intrinsic* properties and lead toward new applications of dielectric oxynitride perovskites.

Acknowledgements

This work was supported in part by a Grant-in-Aid for Scientific Research (A) (Grant #24245039) from the Japan Society for the Promotion of Science (JSPS). The authors thank Ms. D. Chen of Hokkaido University for supply of preliminary thermogravimetric results.

*Corresponding Authors: Y. Masubuchi (yuji-mas@eng.hokudai.ac.jp) and S.-K. Sun (sksun@eng.hokudai.ac.jp)

[a]Faculty of Engineering, Hokkaido University, N13 W8, Kita-ku, Sapporo, 060-8628, Japan. E-mail: yuji-mas@eng.hokudai.ac.jp and sksun@eng.hokudai.ac.jp; Tel: +81-(0)11-706-6742.

Notes and references

1 R. H. Mitchell, in *Perovskites, modern and ancient*, ed. *Almas Press Inc.*, Ontario, 2002.

2 (a) S. G. Ebbinghaus, H.-P. Abicht, R. Dronskowski, T. Müller, A. Reller and A. Weidenkaff, *Prog. Solid State Chem.*, 2009, **37**, 173-205; (b) A. Fuertes, *J. Mater. Chem.*, 2012, **22**, 3293-3299; (c) M. Jansen and H. P. Letschert, *Nature*, 2000, **404**, 980-982.

3 F. Tessier, P. Maillard, F. Chevire, K. Domen and S. Kikkawa, *J. Ceram. Soc. Jpn.*, 2009, **117**, 1-5.

4 (a) A. Fuertes, *Dalton Trans.*, 2010, **39**, 5942-5948; (b) J. P. Attfield, *Cryst. Growth Des.*, 2013, **13**, 4623-4629.

5 (a) M. Yang, J. Oró-Solé, J. A. Rodgers, A. B. Jorge, A. Fuertes and J. P. Attfield, *Nat. Chem.*, 2011, **3**, 47-52; (b) Y.-R. Zhang, T. Motohashi, Y. Masubuchi and S. Kikkawa, *J. Ceram. Soc. Jpn.*, 2011, **119**, 581-586; (c) S. H. Porter, Z. Huang and P. M. Woodward, *Cryst. Growth Des.*, 2014, **14**, 117-125.

6 (a) D. Logvinovich, J. Hejtmánek, K. Knížek, M. Maryško, N. Homazava, P. Tomeš, R. Aguiar, S. G. Ebbinghaus, A. Reller and A. Weidenkaff, *J. Appl. Phys.*, 2009, **105**, 023522; (b) J. Oro-Sole, L. Clark, W. Bonin, J. P. Attfield and A. Fuertes, *Chem. Commun.*, 2013, **49**, 2430-2432; (c) M. Yang, J. Oró-Solé, A. Kusmartseva, A. Fuertes and J. P. Attfield, *J. Am. Chem. Soc.*, 2010, **132**, 4822-4829; (d) A. Kusmartseva, M. Yang, J. Oró-Solé, A. M. Bea, A. Fuertes and J. P. Attfield, *Appl. Phys. Lett.*, 2009, **95**, 022110; (e) A. B. Jorge, J. Oró-Solé, A. M. Bea, N. Mufti, T. T. M. Palstra, J. A. Rodgers, J. P. Attfield and A. Fuertes, *J. Am. Chem. Soc.*, 2008, **130**, 12572-12573.

7 X. Gouin, R. Marchand, Y. Laurent and F. Gervais, *Solid State Commun.*, 1995, **93**, 857-859.

8 Y.-I. Kim, P. M. Woodward, K. Z. Baba-Kishi and C. W. Tai, *Chem. Mater.*, 2004, **16**, 1267-1276.

9 (a) Y.-R. Zhang, T. Motohashi, Y. Masubuchi and S. Kikkawa, *J. Eur. Ceram. Soc.*, 2012, **32**, 1269-1274; (b) Y. R. Zhang, Y. Masubuchi, T. Motohashi, S. Kikkawa and K. Hirota, *Ceram. Int.*, 2013, **39**, 3377-3380; (c) S.-K. Sun, Y.-R. Zhang, Y. Masubuchi, T. Motohashi and S. Kikkawa, *J. Am. Ceram. Soc.*, 2014, **97**, 1023-1027.

10 (a) C. Le Paven-Thivet, L. Le Gendre, J. Le Castrec, F. Cheviré, F. Tessier and J. Pinel, *Prog. Solid State Chem.*, 2007, **35**, 299-308; (b) A. Ziani, C. Le Paven-Thivet, L. Le Gendre, D. Fasquelle, J. C. Carru, F. Tessier and J. Pinel, *Thin Solid Films*, 2008, **517**, 544-549; (c) C. Le Paven-Thivet, A. Ishikawa, A. Ziani, L. Le Gendre, M. Yoshida, J. Kubota, F. Tessier and K. Domen, *J. Phys. Chem., C*, 2009, **113**, 6156-6162; (d) A. Ziani, C. Le Paven-Thivet, D. Fasquelle, L. Le Gendre, R. Benzerga, F. Tessier, F. Cheviré, J. C. Carru and A. Sharaiha, *Thin Solid Films*, 2012, **520**, 4536-4540; (e) Y. Lu, C. Le Paven-Thivet, R. Benzerga, L. Le Gendre, A. Sharaiha, F. Tessier and F. Cheviré, *Appl. Surf. Sci.*, 2013, **264**, 533-537; (f) Y. Lu, C. Le Paven, H. V. Nguyen, R. Benzerga, L. Le Gendre, S. Rioual, F. Tessier, F. Cheviré, A. Sharaiha, C. Delaveaud and X. Castel, *Cryst. Growth Des.*, 2013, **13**, 4852-4858.

11 D. Oka, Y. Hirose, H. Kamisaka, T. Fukumura, K. Sasa, S. Ishii, H. Matsuzaki, Y. Sato, Y. Ikuhara and T. Hasegawa, *Sci. Rep.*, 2014, **4**, 4987.

12 R. Aguiar, D. Logvinovich, A. Weidenkaff, A. Reller and S. G. Ebbinghaus, *Thermochim. Acta*, 2008, **471**, 55-60.

13 Y. Masubuchi, F. Kawamura, T. Taniguchi and S. Kikkawa, *J. Eur. Ceram. Soc.*, [doi:10.1016/j.jeurceramsoc.2014.10.028].

14 (a) S.-K. Sun, T. Motohashi, Y. Masubuchi and S. Kikkawa, *J. Eur. Ceram. Soc.*, 2014, **34**, 4451-4455; (b) S.-K. Sun, Y. Masubuchi, T. Motohashi and S. Kikkawa, *J. Eur. Ceram. Soc.*, [doi:10.1016/j.jeurceramsoc.2014.11.019].

15 B. Eck, R. Dronskowski, M. Takahashi and S. Kikkawa, *J. Mater. Chem.*, 1999, **9**, 1527-1537.

16 (a) F. Tessier, A. Navrotsky, R. Niewa, A. Leineweber, H. Jacobs, S. Kikkawa, M. Takahashi, F. Kanamaru and F. J. DiSalvo, *Solid State Sci.*, 2000, **2**, 457-462; (b) A. Nagatomi, S. Kikkawa, T. Hinomura, S. Nasu and F. Kanamaru, *J. Jpn Soc. Powder and Powder Metall.*, 1999, **46**, 151-155; (c) S. Kikkawa, A. Yamada, Y. Masubuchi and T.

Takeda, *Mater. Res. Bull.*, 2008, **43**, 3352-3357; (d) K. Yamanaka, Y. Onuma, S. Yamashita, Y. Masubuchi, T. Takeda and S. Kikkawa, *J. Solid State Chem.*, 2010, **183**, 2236-2241; (e) S. Yamashita, Y. Masubuchi, Y. Nakazawa, T. Okayama, M. Tsuchiya and S. Kikkawa, *J. Solid State Chem.*, 2012, **194**, 76-79.

17 (a) Y. Kawaai, A. Yamada, T. Takeda and S. Kikkawa, *Jpn. J. Appl. Phys.*, 2004, **43**, 5671-5672; (b) R. Saito, Y. Masubuchi, T. Motohashi, S. Kikkawa and M. Sasaki, *Mater. Res. Bull.*, 2011, **46**, 547-550.

18 A. Miyaake, Y. Masubuchi, T. Takeda, T. Motohashi and S. Kikkawa, *Dalton Trans.*, 2010, **39**, 6106-6111.

19 Y. Hinuma, H. Moriwake, Y.-R. Zhang, T. Motohashi, S. Kikkawa and I. Tanaka, *Chem. Mater.*, 2012, **24**, 4343-4349.

20 L. Clark, J. Oró-Solé, K. S. Knight, A. Fuertes and J. P. Attfield, *Chem. Mater.*, 2013, **25**, 5004-5011.

21 (a) P. Antoine, R. Marchand, Y. Laurent, C. Michel and B. Raveau, *Mater. Res. Bull.*, 1988, **23**, 953-957; (b) R. Pastrana-Fábregas, J. Isasi-Marín, C. Cascales and R. Sáez-Puche, *J. Solid State Chem.*, 2007, **180**, 92-97; (c) P. Antoine, R. Assabaa, P. L'Haridon, R. Marchand, Y. Laurent, C. Michel and B. Raveau, *Mater. Sci. Eng. B*, 1989, **5**, 43-46; (d) P. Maillard, F. Tessier, E. Orhan, F. Cheviré and R. Marchand, *Chem. Mater.*, 2004, **17**, 152-156; (e) A. Hellwig and A. Hendry, *J. Mater. Sci.*, 1994, **29**, 4686-4693.

22 (a) H. J. Lee, J.-G. Choi, C. W. Colling, M. S. Mudholkar and L. T. Thompson, *Appl. Surf. Sci.*, 1995, **89**, 121-130; (b) J. J. Vajo, W. Tsai, and W. H. Weinberg, *J. Phys. Chem.*, 1985, **89**, 3243-3251.

23 Y. Mizuno, H. Wagata, K. Yubuta, N. Zettsu, S. Oishi and K. Teshima, *CrystEngComm*, 2013, **15**, 8133-8138.

24 G. Liu, X. Zhao and H. A. Eick, *J. Alloys Compd.*, 1992, **187**, 145-156.

25 (a) Y.-I. Kim, *Ceram. Int.*, 2014, **40**, 5275-5281; (b) F. Tessier, L. Le Gendre, F. Cheviré, R. Marchand and A. Navrotsky, *Chem. Mater.*, 2005, **17**, 3570-3574; (c) E. Günther, R. Hagenmayer and M. Jansen, *Z. Anorg. Allg. Chem.*, 2000, **626**, 1519-1525; (d) M. Matsukawa, R. Ishikawa, T. Hisatomi, Y. Moriya, N. Shibata, J. Kubota, Y. Ikuhara and K. Domen, *Nano Lett.*, 2014, **14**, 1038-1041.

26 (a) S. Balaz, S. H. Porter, P. M. Woodward and L. J. Brillson, *Chem. Mater.*, 2013, **25**, 3337-3343; (b) J. Grins and G. Svensson, *Mater. Res. Bull.*, 1994, **29**, 801-809.

27 B. L. Cushing, V. L. Kolesnichenko and C. J. O'Connor, *Chem. Rev.*, 2004, **104**, 3893-3946.

28 T. Motohashi, Y. Hamade, Y. Masubuchi, T. Takeda, K. Murai, A. Yoshiasa and S. Kikkawa, *Mater. Res. Bull.*, 2009, **44**, 1899-1905.

29 A. Rachel, S. G. Ebbinghaus, M. Güngerich, P. J. Klar, J. Hanss, A. Weidenkaff and A. Reller, *Thermochim. Acta*, 2005, **438**, 134-143.

30 D. Segal, *J. Mater. Chem.*, 1997, **7**, 1297-1305.

31 A. Gomathi, S. Reshma and C. N. R. Rao, *J. Solid State Chem.*, 2009, **182**, 72-76.

32 Z. K. Huang, D. S. Yan, T. S. Yen and T. Y. Tien, *J. Solid State Chem.*, 1990, **85**, 51-55.

33 S. J. Clarke, K. A. Hardstone, C. W. Michie and M. J. Rosseinsky, *Chem. Mater.*, 2002, **14**, 2664-2669.

34 D. Li, W. Li, C. Fasel, J. Shen and R. Riedel, *J. Alloys Compd.*, 2014, **586**, 567-573.

35 B. Ravel, Y. I. Kim, P. M. Woodward and C. M. Fang, *Phys. Rev. B*, 2006, **73**, 184121.

36 Y.-I. Kim, W. Si, P. M. Woodward, E. Sutter, S. Park and T. Vogt, *Chem. Mater.*, 2007, **19**, 618-623.

37 (a) P. Lunkenheimer, V. Bobnar, A. V. Pronin, A. I. Ritus, A. A. Volkov and A. Loidl, *Phys. Rev. B*, 2002, **66**, 052105; (b) M. Fujimoto and W. D. Kingery, *J. Am. Ceram. Soc.*, 1985, **68**, 169-73.

38 N. Uchida, M. Koizumi, and M. Shimada, *J. Am. Ceram. Soc.*, 1985, **68**, c38-c40.

39 S. G. Ebbinghaus, R. Aguiar, A. Weidenkaff, S. Gsell and A. Reller, *Solid State Sci.*, 2008, **10**, 709-716.

40 A. E. Ringwood, and M. Seabrook, *J. Geophys. Res.*, 1963, **68**, 4601-4609.

41 (a) Y. Matsuo, H. Sasaki, S. Hayakawa, F. Kanamaru and M. Koizumi, *J. Am. Ceram. Soc.*, 1969, **52**, 516-517; (b) K. Kitada, M. Kobune, W. Adachi, T. Yazawa, H. Saitoh, K. Aoki, J. Mizuki, K. Ishikawa, Y. Hiranaga and Y. Cho, *Chem. Lett.*, 2008, **37**, 560-561; (c) M. Akaogi, H. Kojitani, H. Yusa, R. Yamamoto, M. Kido and K. Koyama, *Phys. Chem. Miner.*, 2005, **32**, 603-613.

42 (a) D. A. Dzivenko, A. Zerr, G. Miehe and R. Riedel, *J. Alloys Compd.*, 2009, **480**, 46-49; (b) B. L. Chamberland, *Mater. Res. Bull.*, 1971, **6**, 311-315.

43 I. Troyanchuk, N. V. Kasper, O. S. Mantytskaya and E. F. Shapovalova, *Mater. Res. Bull.*, 1995, **30**, 421-425.

44 R. Marchand, F. Pors and Y. Laurent, *Rev. Int. Hautes Temp. Réfract.*, 1986, **23**, 11-15.

45 M. Yang, J. A. Rodgers, L. C. Middler, J. Oró-Solé, A. B. Jorge, A. Fuertes and J. P. Attfield, *Inorg. Chem.*, 2009, **48**, 11498-11500.

46 (a) I. Kinski, G. Miehe, G. Heymann, R. Theissmann, R. Riedel and H. Huppertz, *Z. Naturforsch*. 2005, **60b**, 831-836; (b) H. Huppertz, S. A. Hering, C. E. Zvoriste, S. Lauterbach, O. Oeckler, R. Riedel and I. Kinski, *Chem. Mater.*, 2009, **21**, 2101-2107.

47 S. Porowski, *J. Cryst. Growth*, 1996, **166**, 583-589.

48 F. Kawamura, K. Watanabe, T. Takeda and T. Taniguchi, *J. Cryst. Growth*, 2011, **321**, 100-105.

49 (a) F. Kanamaru, H. Miyamoto, Y. Mimura, M. Koizumi, M. Shimada, S. Kume and S. Shin, *Mater. Res. Bull.*, 1970, **5**, 257-261; (b) Y. Shirako, H. Kojitani, M. Akaogi, K. Yamaura and E. Takayama-Muromachi, *Phys. Chem. Miner.*, 2009, **36**, 455-462.

50 (a) F. P. Bundy, H. P. Bovenkerk, H. M. Strong and R. H. Wentorf Jr., *J. Chem. Phys.*, 1961, **35**, 383-391; (b) R. C. DeVries and J. F. Fleischer, *J. Cryst. Growth*, 1972, **13–14**, 88-92.

51 (a) H. D. Stromberg and D. R. Stephens, *Am. Ceram. Soc. Bull.*, 1970, **49**, 1031-1032; (b) T. Yamada, M. Shimada and M. Koizumi, *Am. Ceram. Soc. Bull.*, 1981, **60**, 1281-1283, 1288; (c) J. S. Nadeau, *Am. Ceram. Soc. Bull.*, 1973, **52**, 170-174; (d) K. Takagi, M. Akada, K. Ozaki, N. Kobayashi, T. Ogawa, Y. Ogata, and M. Takahashi, *J. Appl. Phys.*, 2014, **115**, 103905; (e) T. Taniguchi, M. Akaishi and S. Yamaoka, *J. Mater. Res.*, 1999, **14**, 162-169.

52 K. Leinenweber, W. Utsumi, Y. Tsuchida, T. Yagi and K. Kurita, *Phys. Chem. Miner.*, 1991, **18**, 244-250.

53 T. Locherer, D. Frost and H. Fuess, *J. Solid State Chem.*, 2008, **181**, 2983-2988.

54 (a) W. R. Matizamhuka, M. Herrmann, I. Sigalas and K. Sempf, *J. Am. Ceram. Soc.*, 2007, **90**, 2280-2282; (b) W. R. Matizamhuka, I. Sigalas and M. Herrmann, *Ceram. Int.*, 2008, **34**, 1481-1486.

55 (a) N. Schönberg, *Acta Chem. Scand.*, 1954, 8, 240-245; (b) G. Brauer and W. Kiliani, *Z. Anorg. Allg. Chem.*, 1979, **452**, 17-26.

56 Y. Cohen and I. Riess, *Mater. Sci. Eng. B*, 1994, **25**, 197-202.
57 Y. Lu, A. Ziani, C. Le Paven-Thivet, R. Benzerga, L. Le Gendre, D. Fasquelle, H. Kassem, F. Tessier, V. Vigneras, J. C. Carru and A. Sharaiha, *Thin Solid Films*, 2011, **520**, 778-783.
58 D. Fasquelle, A. Ziani, C. Le Paven-Thivet, L. Le Gendre and J. C. Carru, *Mater. Lett.*, 2011, **65**, 3102-3104.
59 (a) D. Oka, Y. Hirose, T. Fukumura and T. Hasegawa, *Cryst. Growth Des.*, 2013, **14**, 87-90; (b) R. Aguiar, D. Logvinovich, A. Weidenkaff, H. Karl, C. W. Schneider, A. Reller and S. G. Ebbinghaus, *Mater. Res. Bull.*, 2008, **43**, 1376-1383.